IEEE Access
Multidisciplinary | Rapid Review | Open Access Journal

SPECIAL SECTION ON ARTIFICIAL INTELLIGENCE (AI)-EMPOWERED INTELLIGENT TRANSPORTATION SYSTEMS

Received December 21, 2019, accepted January 4, 2020, date of publication January 9, 2020, date of current version January 21, 2020.

Digital Object Identifier 10.1109/ACCESS.2020.2965186

Contour-Maintaining-Based Image Adaption for an Efficient Ambulance Service in Intelligent Transportation Systems

QINGFANG LIU[1,2], BAOSHENG KANG[1], KEPING YU[3,4], (Member, IEEE), XIN QI[3], JING LI[5], SHOUJIN WANG[6], AND HONG-AN LI[7]

[1]School of Information Science and Technology, Northwest University, Xi'an 710127, China
[2]Information and Network Center, Training Center of China Post Group, Shijiazhuang 050021, China
[3]Global Information and Telecommunication Institute, Waseda University, Tokyo 169-8050, Japan
[4]Shenzhen Boyi Technology Company Ltd., Shenzhen 518125, China
[5]School of Information Engineering, Nanchang University, Nanchang 330031, China
[6]Department of Computing, Macquarie University, Sydney, NSW 2113, Australia
[7]College of Computer Science and Technology, Xi'an University of Science and Technology, Xi'an 710054, China

Corresponding author: Keping Yu (keping.yu@aoni.waseda.jp)

This work was supported in part by the Natural Science Basic Research Plan in Shaanxi Province of China under Grant 2019JM-162, in part by the Doctoral Research Startup Foundation of Xi'an University of Science and Technology under Grant 2019QDJ007, in part by the National Natural Science Foundation of China under Grant 61703198 and Grant 61963027, in part by the Natural Science Foundation for Distinguished Young Scholars of Jiangxi Province under Grant 2018ACB21014, and in part by the Japan Society for the Promotion of Science (JSPS) Grants-in-Aid for Scientific Research (KAKENHI) under Grant JP18K18044.

ABSTRACT Ambulance services play a vital role in intelligent transportation systems (ITS). In an intelligent ambulance system, the medical images can help doctors quickly and accurately understand the patients' condition during first aid. On various display devices in different kinds of ambulances, content-aware image adaption can be used to better present the medical image among different display resolutions and aspect ratios. Most existing methods mainly focus on visual protection of salient areas, such as specific organ parts of the human body, with less attention paid to the visual effect of unimportant areas. However, the human visual system is more sensitive to the edge and contour of images, which are important for ambulance services. To improve the visual effect of adapted images, a contour-maintaining-based image adaption method for an efficient ambulance service in ITS is proposed here. Firstly, the proposed method innovatively combines the weighted gradient, saliency, and edge maps into an importance map. Secondly, energy is optimized for reducing contour distortion and interruption according to the visual slope and curvature of contours and edges in non-salient areas. Finally, applying the sub-procedure of a forward seam carving method, the optimal seams can more evenly pass through the contour areas. The experimental results demonstrate that the proposed method is more effective than other similar methods.

INDEX TERMS Medical image adaption, ambulance mounted, intelligent system, contour-maintaining, seam carving.

I. INTRODUCTION

With the rapid development of computer-aided diagnosis technology [1], a variety of medical imaging technologies have emerged clinically for capturing medical images of human internal tissues and organs, such as Computed Tomography (CT), Nuclear Magnetic Resonance Imaging (NMRI), and Ultrasound Imaging (UI). In the ambulance, these medical images can now be presented on ambulance-mounted intelligent systems for fast and accurate diagnosis with the development of artificial intelligence technology [2]–[4], mobile communication technology [5]–[8], the and Internet of Things [9]–[11]. However, the pixels of these medical images have been already fixed in the process of image production. To be displayed properly on different display devices, such as computer screens, projectors, notebooks, tablets, smart phones, and intelligent systems in vehicles, these medical images need to be adjusted to suit different

The associate editor coordinating the review of this manuscript and approving it for publication was Amr Tolba.

display resolutions and aspect ratios. The process of image adjustment is also called image retargeting or image adaptation [12]. Traditional adaptation methods, mainly including uniform scaling and direct cropping, only consider the original size and the target size of images, without considering image content; their effects are unsatisfactory. To improve image adaption performance, researchers are paying more attention to content-aware adaptation techniques, which are mainly classified into three types: discrete, continuous, and multi-operational adaption.

Discrete adaption methods mainly refer to seam carving. Avidan and Shamir [13] introduced the concept of seam carving. To achieve image adaptation, the seam carving adapting method inserts or deletes eight-connected pixels paths by defining the energy minimization equation in a gradient map. Rubinstein et al. [14] used the graph cut method to find the path with the least energy. Considering the newly added energy after deleting the pixels, they proposed a forward seam carving method, different from backward seam carving [13], which only considers the energy of the pixels themselves. Wang and Yuan [15] used a super-resolution method to improve the quality of the adapted image. Zhang et al. [16] adopted a down-sampled thumbnail technique to accelerate seam carving.

Continuous adaptation methods mainly include mesh deformation. The main idea of mesh deformation is to firstly divide the input image into a mesh grid. Secondly, the importance of each mesh is calculated according to the image content. Finally, the deformation occurs, as much as possible, in the less important mesh areas during the adaptation process. Thus, the important mesh areas are unchanged or proportional. Scholars have used various mesh shapes to segment images into small pieces, such as triangles [17], [18] and quadrilaterals [19], [20].

The multi-operation adaptation methods [21], [22] produce slightly better results by combining the specific sequence and number of methods, such as seam carving, scaling,and cropping, when the single method fails. However, its effectiveness cannot be evidently improved, and its efficiency is poor.

Most studies focused only on the display quality of salient regions, whereas less attention has been paid to the adaption effect and display quality of unimportant regions. However, the human visual system is more sensitive to edge and contour [23]. With regard to the contours in unimportant areas, distortion and deformation produce unpleasant display defects and fade the visual effect of the adapted image.

This paper proposes a high-quality medical image adaptation method based on contour preservation for ambulance-mounted intelligent system. This method protects the integrity and display proportion of prominent object, improves the continuity and smoothness of edges and contours, and maintains their shape in non-salient areas. Ultimately, the method can reduce distortion and artificial noise and enhance the quality of image adaption. Experiments showed that the proposed method can improve the visual effect of unimportant areas, reduce visual bias, and ultimately improve the overall display quality of adapted images.

The rest of this paper is organized as follows: Section 2 presents the proposed contour-maintaining-based medical image adaption method. The experiment used to verify the effectiveness and a discussion are provided in Section 3. Conclusions are outlined in Section 4.

II. PROPOSED METHOD

The flow chart of the proposed approach is illustrated in Figure 1. Its framework includes three steps: (1) generating an importance map through the weighted combination of gradient, saliency, and edge maps to create a basic energy map; (2) optimizing the energy map using the visual characteristics of curve inclination and bending degree; and (3) performing forward seam carving operation to achieve image adaptation.

A. IMPORTANCE MAP

An importance map is used to measure the importance of image content. The width and height of the importance map are the same as the input image. The higher the importance of pixel, the greater the value of corresponding position.

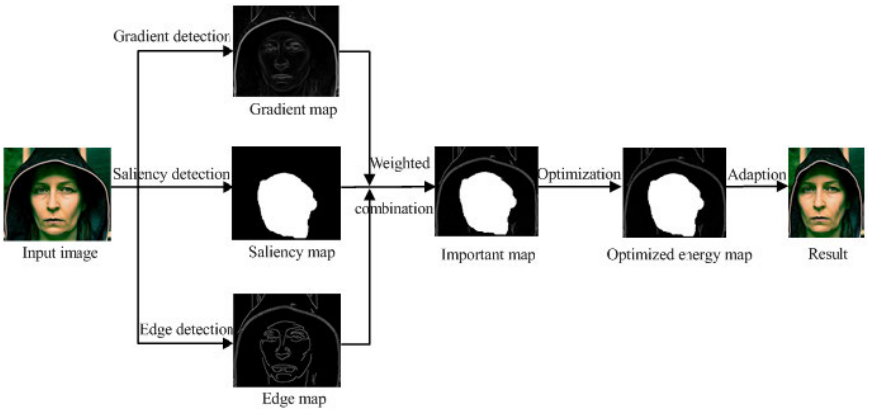

FIGURE 1. Flow chart of the proposed contour-maintaining-based image adaption method.

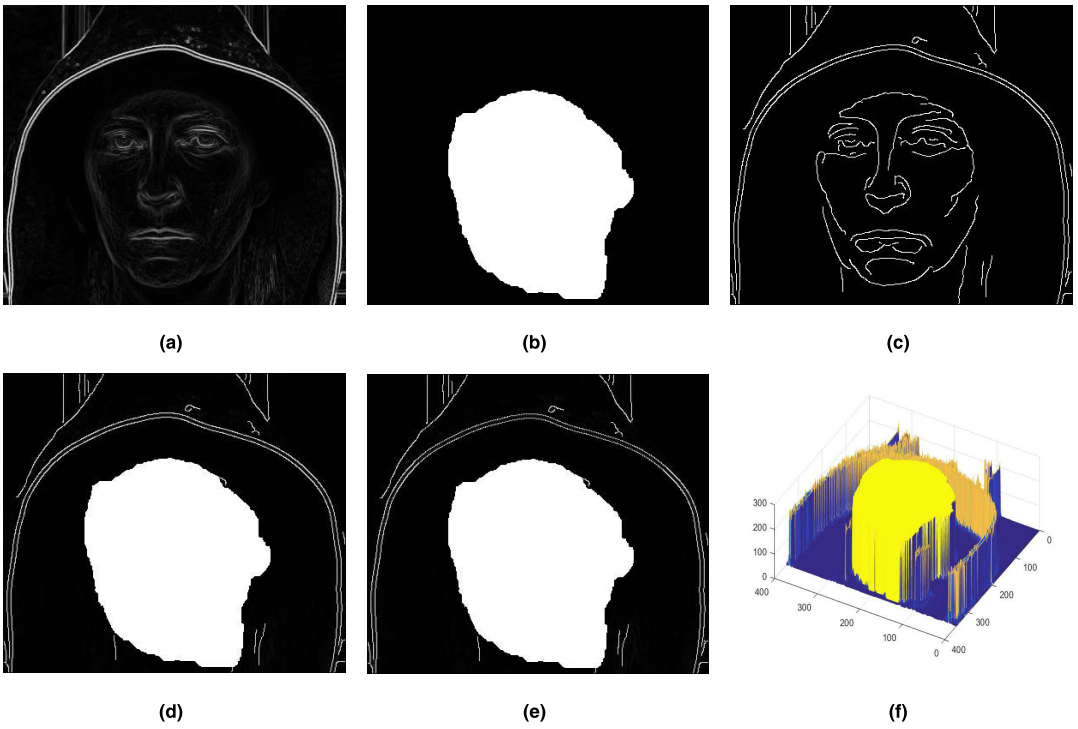

FIGURE 2. An example of the importance map and energy map production: (a) gradient map, (b) saliency map, (c) edge map, and (d) importance map generated by weighted combination of (a-c). (e) Energy map refined from (d). (f) Three-dimensional (3D) effect of refined energy map (e).

An importance map is generated by combining the weighted gradient, saliency, and edge maps.

A gradient map reflects the variation degree between a pixel and its neighbors.

A saliency map highlights a prominent object or interesting areas of the input image using saliency detection. For medical images, the methods based on region growing [24], probabilistic atlases [25], and graph cut [26] can be used to separate organ regions of interest. Various morphological methods can also be combined to obtain the salient parts. For general images, Itti et al. [27] introduced a visual attention calculation model guided by a biological cognitive system that mainly focuses on the prominent part of the whole picture. Hou and Zhang [28] used spectrum-based visual attention mechanisms to remove background information and highlight salient parts. Cheng et al. [29] proposed a fast and robust method for detecting visual saliency regions based on global contrast analysis, which can quickly and effectively identify and segment the saliency regions.

An edge map represents contours and edges separated from input images. Canny [30] edge detection methods can produce clearer and better edges than others, such as Sobel, Roberts, and Prewitt edge detection. In this study, Canny edge detection was adopted to generate edge map.

The importance map I_{im} (Figure 2d) was generated by the weighted combination of the normalized gradient map I_g, saliency map I_s, and edge map I_e (Figures 2a–c).

The importance map I_{im} is defined as:

$$I_{im}(X,Y) = Max\{\alpha \times I_s(X,Y), \beta \times I_b(X,Y), \gamma \times I_g(X,Y)\}, \quad (1)$$

where the values of weight coefficient $\alpha, \beta,$and γ are set to 1, 0.8, and 0.2, respectively.

Examples of an importance map and an energy map production are depicted in Figure 2.

B. CONTOUR-MAINTAINING-BASED ENERGY OPTIMIZATION

The importance map was used as the basic energy diagram, and an accurate energy map was obtained by optimization. The core idea of the algorithm is optimizing the energy of the edge areas based on the tangent slope (inclination degree) and curvature (curvature degree) of the contour areas in the non-salient areas of the image.

1) EDGE POINT SERIALIZATION

The points in the edge map are discrete and disorderly. We used the boundary tracking method [31] for serialization, which views the edges as objects.

The number of points on the Lth edge is N_L in the non-salient regions. The edge with an N_L not higher than the threshold N_T ($N_T = 20$) can barely attract human visual attention. So, the energy of these points was directly set to

a lower value. The updated lower energy E_{lower} is calculated as:

$$E_{lower} = E/5, \quad \text{s.t. NL} \leq 20. \tag{2}$$

Edges with more than N_L points more easily attract visual attention, and the energy of these edges needs to be further optimized.

2) SLOPE CALCULATION

The slope of the tangent at one point on the curve, which reflects the steepness of the tangent at this point, can be obtained from the first-order difference.

On the Lth edge, the coordinates of the a th ($1 \leq a \leq N_L$) point is defined as (X_a, Y_a). At point (X_a,Y_a), the slope K_a is defined as:

$$K_a = -\frac{(X_{a+1} - X_{a-1})}{(Y_{a+1} - Y_{a-1})}. \tag{3}$$

Because the image pixels are discrete points, directly calculating slope and curvature with one or two adjacent points will lead to jumps in the results and cannot reflect the overall trend of the line. Thus, a multi-point weighted method should be adopted to calculate the slope and curvature.

The multi-point weighted slope K_a^* at point (X_a,Y_a) is defined as:

$$K_a^* = -\frac{\sum_{i=1}^{3} w_i \times (X_{a+i} - X_{a-i})}{\sum_{i=1}^{3} w_i \times (Y_{a+i} - Y_{a-i})}, \tag{4}$$

where the values of weight coefficients w_1, w_2,and w_3 are set to 3, 2, and 1, respectively.

3) CURVATURE CALCULATION

Curvature [32] reflects the bending degree of the curve at one point. Curvature κ is expressed as:

$$\kappa = \left| \frac{d\alpha}{ds} \right|, \tag{5}$$

where $d\alpha$ is the differential of the tangent angle variation and ds is the differential of the arc length of the curve.

With the arc tangent function, the angle θ between the tangent at point (X_a,Y_a) and the horizontal line can be calculated as $\arctan(K_a^*)$. The differential of the tangent angle variation $d\alpha$ can be approximately computed as:

$$d\alpha \approx \Delta\theta = \arctan(K_{a+1}^*) - \arctan(K_a^*). \tag{6}$$

The Euclidean distance between point (X_{a+1},Y_{a+1}) and point (X_a,Y_a) can be regarded as the differential of the arc length in the process of curvature calculation. So, the differential of arc length ds can be approximately computed as:

$$ds \approx \Delta\text{s} = \sqrt{(X_{a+1} - X_a)^2 + (Y_{a+1} - Y_a)^2}. \tag{7}$$

Then, the approximate curvature κ^* at point (X_a,Y_a) can be calculated as:

$$\kappa_a^* \approx \left| \frac{\Delta\theta}{\Delta\text{s}} \right| = \left| \frac{\arctan(K_{a+1}^*) - \arctan(K_a^*)}{\sqrt{(X_{a+1} - X_a)^2 + (Y_{a+1} - Y_a)^2}} \right|. \tag{8}$$

Additionally, when the edge is excessively bending, the difference in the arc tangent function will not correctly reflect the included angle between the two tangent lines because the range of the arc tangent function is ($-\pi/2$,$\pi/2$). Then, the cosine theorem is used to compute the included angle θ^* between two connections among three points. The first connection exists between point (X_a,Y_a) and weighted coordinate point (X_{a+},Y_{a+}), and the second connection occurs between point (X_a,Y_a) and weighted coordinate point (X_{a-},Y_{a-}). The weighted coordinate points (X_{a+},Y_{a+}) and (X_{a-},Y_{a-}) are defined as:

$$X_a^+ = \frac{\sum_{i=1}^{3} w_i \times X_{a+i}}{\sum_{i=1}^{3} w_i}, \quad Y_a^+ = \frac{\sum_{i=1}^{3} w_i \times Y_{a+i}}{\sum_{i=1}^{3} w_i}, \tag{9}$$

$$X_a^- = \frac{\sum_{i=1}^{3} w_i \times X_{a-i}}{\sum_{i=1}^{3} w_i}, \quad Y_a^- = \frac{\sum_{i=1}^{3} w_i \times Y_{a-i}}{\sum_{i=1}^{3} w_i}, \tag{10}$$

where the values of weighted coefficients w_1, w_2,and w_3 are set to 3, 2, and 1, respectively.

As a basis for judging whether the curve is excessively bending, the included angle θ^* is defined as:

$$\theta^* = \arccos\left(\frac{A^2 + B^2 - C^2}{2AB}\right), \tag{11}$$

where:

$$A = \sqrt{(X_a - X_a^-)^2 + (Y_a - Y_a^-)^2},$$
$$B = \sqrt{(X_a^+ - X_a)^2 + (Y_a^+ - Y_a)^2}. \tag{12}$$

4) ENERGY OPTIMIZATION

The flow chart of the four steps of the proposed energy optimization is illustrated in Figure 3.

Step 1: The curvature κ of curve is used to judge whether the curve is excessively bending. When κ is larger than the threshold κ_T ($\kappa_T = 0.1$) and the included angle θ^* is smaller than the threshold θ_T^* ($\theta_T^* = 0.75\pi$), the curve bending degree at this point is large, and the higher energy does not need to be changed. Otherwise, the curve near this point has a smaller bending degree, and proceed to step 2.

Step 2: If the absolute value of slope $|K|$ is greater than the threshold K_T ($K_T = 1$), the edge at this point is steeper. If the seam passes through the point, the point will be deleted. This will cause greater visual distortion. So, the higher energy of the point will remain unchanged. Otherwise, the edge at the point will not only be slightly bending but also be relatively gentle, and proceed to step 3.

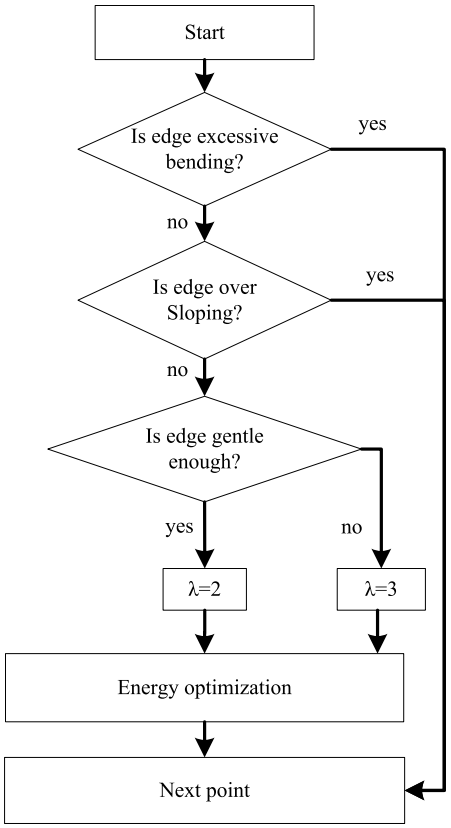

FIGURE 3. Flow chart of energy optimization.

Step 3: This step judges the slope gentleness at the point according to the slope. If the absolute value of the slope $|K|$ is not less than the threshold K_p ($K_p = 0.5$), the value of period λ is set to 3, then proceed to step 4 to optimize the energy. Otherwise, the value of period λ is set to 2, and proceed to step 4 to optimize the energy. Thus, the period λ is defined as:

$$\lambda = \begin{cases} 2, & \text{if } 0 \le |\mathrm{K}| < \mathrm{K_P}, \\ 3, & \text{if } \mathrm{K_P} \le |\mathrm{K}| < \mathrm{K_T}. \end{cases} \tag{13}$$

Step 4: This is the core step used to optimize the energy. Zigzag energy forms along the contour by periodically adjusting the value of energy at a point (X_a, Y_a) and the adjacent points (X_{a+1}, Y_a), (X_{a-1}, Y_a). The smaller the tangent slope, the greater the degree of energy adjustment. When $|K|$ is 0, the updated energy is reduced to one-half of the original energy to the greatest extent. When $|K|$ is 1, the original energy remains unchanged. By updating the original energy E, the optimized energy E^* is defined as:

$$E^* = E - \frac{E}{2} \times (1 - |K|) = E \times (\frac{1}{2} + \frac{|K|}{2}). \tag{14}$$

To maintain the shape integrity and continuity of the edges, the energy on the edges should fluctuate periodically to allow the seams to pass through the contour areas evenly. Specifically, at every λ point, the energy must be adjusted. In other words, if the period λ is 2 or 3, one in every two or three points will be selected to update its energy. At point (X_a, Y_a), the optimized energy is defined as:

$$E_a^* = \begin{cases} E_a \times (\frac{1}{2} + \frac{|K|}{2}), & \lambda \bmod a = 0 \\ E, & \text{otherwise.} \end{cases} \tag{15}$$

An example of optimized energy map is shown in Figures 2e,f.

C. ADAPTION METHODOLOGY

We used forward seam carving operation [14] as the subprocedure for image adaptation. The following uses vertical seam carving as an example to illustrate the main implementation process.

The energy of point (i, j) is defined as $e(i, j)$. The backward cumulative energy $M(i, j)$ is defined as:

$$M(i,j) = e(i,j) + \min(M(i-1,j-1), M(i-1,j), M(i-1,j+1)). \tag{16}$$

The forward cumulative energy $M^*(i, j)$ is the energy generated by adding new energy $C(i, j)$ to the backward energy $M(i, j)$. $C(i, j)$ is the new energy generated when nonadjacent pixel points become adjacent after deleting the pixel point (i, j). The new energy C (i, j) is defined as:

$$\begin{cases} C_L(i,j) = |e(i,j+1) - e(i,j-1)| + |e(i-1,j) - e(i,j-1)| \\ C_U(i,j) = |e(i,j+1) - e(i,j-1)| \\ C_R(i,j) = |e(i,j+1) - e(i,j-1)| + |e(i-1,j) - e(i,j+1)|. \end{cases} \tag{17}$$

Thus, the forward cumulative energy $M^*(i, j)$ is:

$$M^*(i,j) = e(i,j) + \min \begin{cases} M(i-1,j-1) + C_L(i,j) \\ M(i-1,j) + C_U(i,j) \\ M(i-1,j+1) + C_R(i,j). \end{cases} \tag{18}$$

Starting from the second row of the energy map, calculate the cumulative energy traverses each point of every row until the last row. The final cumulative energy is the sum of the original energy $e(i, j)$ and the minimum cumulative energy of the previous line of the eight-connected path. After calculating the cumulative energy, the dynamic programming method is used for recall, from the last row to the first row, to find the minimum cumulative energy pixels as the optimal seam.

III. EXPERIMENTAL COMPARISON AND ANALYSIS

To validate the method proposed above, experiments were conducted on a computer with an Intel i5-5200U@2.2GHz CPU and 8 GB RAM. The proposed method was implemented in MATLAB R2016a on Windows.

A. DATA SET

To verify the effectiveness of the proposed algorithm, experiments were conducted on two public data sets: SLIVER07 [33], which has 30 groups of clinical abdominal

CT scans images, widely used in medical image processing; and MSRA10K [29], which is widely used in saliency detection and image adaption and contains a total of 10,000 images.

For each data set, five methods were applied for comparison experiments: unified scaling (scaling), direct cropping (cropping), Traditional Seam Carving (TSC) [14], Seam Carving based on Importance map as Energy graph (SC-IE), and the proposed Seam Carving based on Optimized Energy map (SC-OE) for comparison experiments.

We selected horizontal adaption as an example to illustrate the adaption process. To protect the region of interest, the maximum number of vertical seams was equal to the width of the insignificant area. Horizontal optimal adaption percentage is usually obtained by dividing the proper number of vertical seams by image width. Adaption beyond optimal adaption can be achieved using the scaling method. In the following experiments, we manually calculated the width of insignificant area as the maximum number of seams. The number of vertical seams should not be close to but not higher than the maximum.

B. EVALUATION MEASURE

The results of the experiments were evaluated using subjective and objective evaluation. Subjective evaluation was used to assess the quality of the experimental results by observing them in detail according to experimental objectives. Objective evaluation experiments were designed for fairly evaluating the comparison effect. We organized 20 volunteer participants to score the adapted images processed by different methods. Firstly, the original input images were shown to the participants. Then, the adaption results of five different methods were displayed for the participants. After that, participants scored the results on a scale ranging from 1 to 10, with 1 point indicating poor results, and 10 points indicating excellent results. Finally, the average score of each algorithm was calculated after each participant completed the score independently.

C. SLIVER07 RESULT

To compare the performance of five different image adaptation methods on medical images, two abdominal CT images were randomly selected from the SLIVER07 data set. Since CT images are gray-scale, the SC-IE and proposed SC-OE methods use a morphological approach to generate the saliency map. Firstly, opening and closing operations are separately applied to input images. Then, the union operation is used on the two results obtained in the previous step. Finally, the saliency map is produced using the corroding operation on the union result of the last step.

Figure 4 depicts the input images and adapted results of the five methods. CT-1 images in the first row have a smaller liver area, whereas CT-2 images in the second row have a larger liver area. The horizontal optimal adaption percentage of CT-1 and CT-2 is 15%. Images in column (a) are the original input images. Images in columns (b) to (f) are the results of scaling, cropping, TSC, SC-IE, and the proposed SC-OE adaptation method, respectively. Figure 5 shows the optimal deleted seams of TSC, SC-IE, and the proposed SC-OE methods.

Among the abdominal CT images in Figure 4, liver areas in Figure 4b are narrower than the original images. This illustrates that the distortion occurs within the important area of the image when using the scaling adaption method. In Figure 4c, the body surface area near the left and right side is lost; the content near the image border is deleted using the cropping adaption method. The overall effect in Figure 4d is better than in Figures 4b,c; however, serious distortion and fracture of body surface edge areas occur, and liver areas are deformed slightly. In Figure 4e, no deformation in the liver area is visible, but distortion occurred on body surface edge areas. In Figure 4f, the liver area are completely preserved, and the contour of the body surface is smooth and

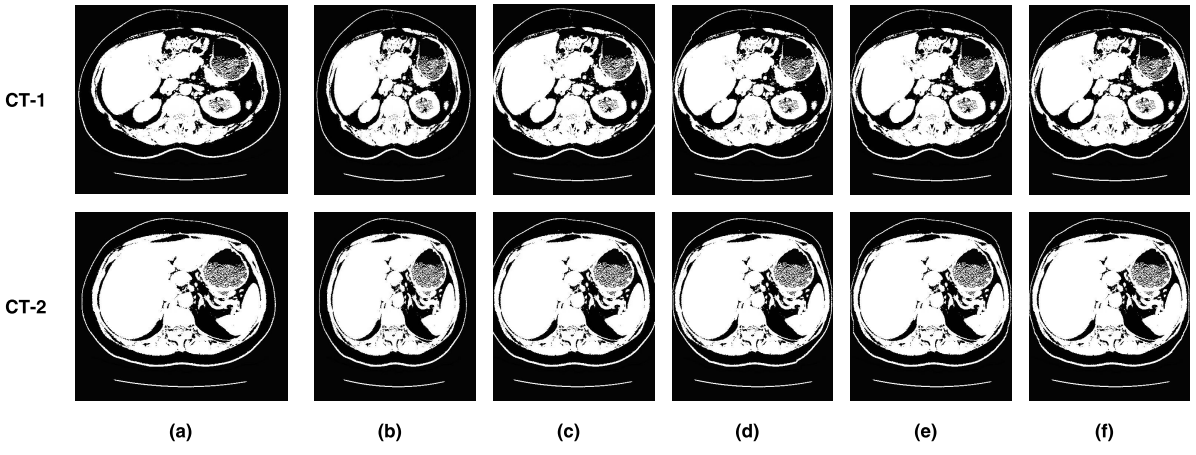

FIGURE 4. Results of comparison experiments on SLIVER07: (a) original input images, and results of (b) scaling, (c) cropping, (d) Traditional Seam Carving (TSC), (e) Seam Carving based on Importance map as Energy graph (SC-IE), and (f) proposed Seam Carving based on Optimized Energy map (SC-OE).

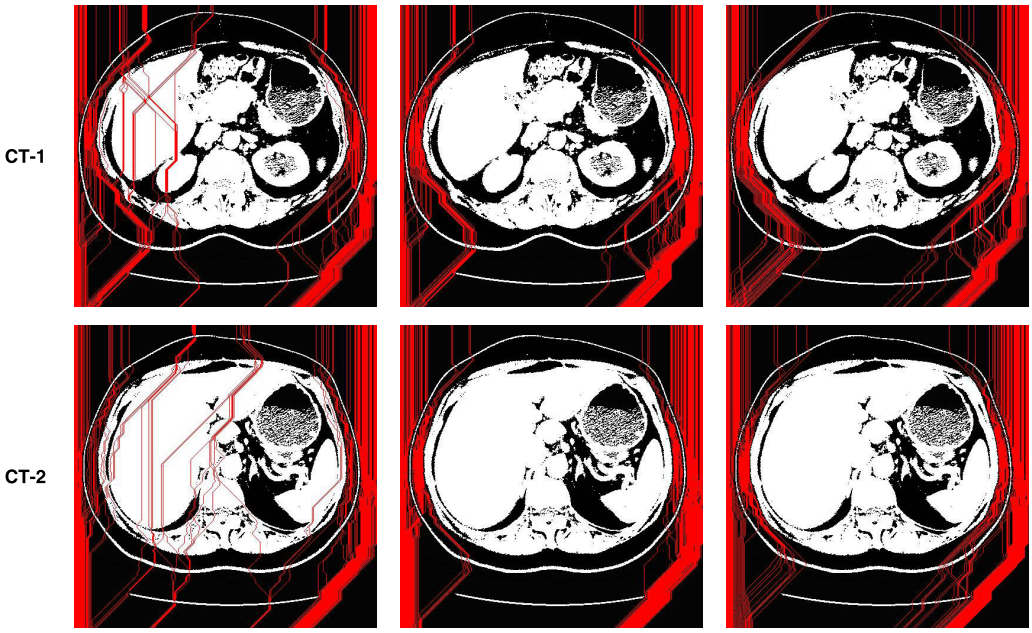

FIGURE 5. Experiments results of optimal seams on SLIVER07. Red lines are the removed seams of (a) TSC, (b) SC-IE, and (c) proposed SC-OE methods.

natural. In conclusion, the image in Figure 4f is obviously more accurate than other methods.

The objective evaluation results of two abdominal CT images of the SLIVER07 data set are provided in Table 1. The average scores of the proposed SC-OE on the two images of SLIVER07 data set were 7.9 and 7.8, which are higher than other methods. Therefore, the results of the proposed SC-OE are more in line with human visual requirements and produce a better visual perception effect.

TABLE 1. Average scores of results for the SLIVER07 data set.

Image	Average scores				
	Scaling	Cropping	TSC	SC-IE	Proposed SC-OE
CT-1	4.1	4.1	7.1	7.6	7.9
CT-2	3.8	4.0	7.0	7.5	7.8

The reasons for these results are as follows. The scaling and cropping methods do not consider the importance of image content, but only focus on the original and target sizes of the image. This leads to an imbalance of the proportions of the liver areas in Figure 4b and information loss of the body surface in Figure 4c. In Figure 4d, the TSC method considers the content of the image, but only depends on the gradient map, which is imprecise. The imprecise evidence results in the seams passing through the liver region, as shown in Figure 5a, as well as excessively distorted contour in body surface areas. In Figure 4e, the SC-IE method uses the importance map as the basis of seam carving, and it comprehensively considers the salient areas and edge areas of the image. However, the energy of the edge areas are not optimized, and seams unevenly pass through the contour regions (Figure 5b), resulting in distortion of the edge in unimportant areas. In Figure 4f, the proposed SC-OE method optimizes the energy map according to the content importance of images and contour characteristics in unimportant areas. As shown in Figure 5c, the proposed SC-OE preserves the salient areas benefited by high energy in the saliency area, and ensures the smoothness and continuity of contour edge by setting periodic and serrated energy in edge areas to lead the optimal seams to evenly pass through the contour area in the non-salient region. In short, scaling and cropping do not consider the importance of image content. TSC only depends on an imprecise gradient map. SC-IE does not apply an energy optimization procedure. SC-OE is built on a precise importance map and contour-maintaining-based energy optimization. So, the visual effect in Figure 4f, which depicts the results of the proposed SC-OE method, is more accurate than the results of other methods.

D. RESULT ON MSRA10K

For comparing the effect of five different image adaptation methods on general images, two images were randomly selected from the MSRA10K data set, and the horizontal optimal adaption percentage of "Head" and "Toy" is 25%. In this study, the SC-IE and proposed SC-OE methods used a previously reported approach [29] to obtain the saliency map. Figure 6 shows the original input images and the adapted results of the five adaption methods. The images in column (a) are the original input images, while images

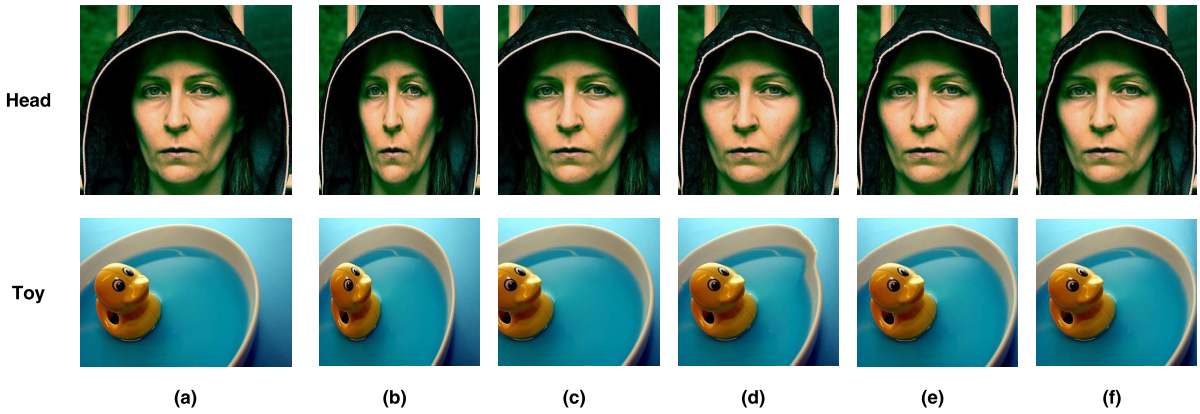

FIGURE 6. Results of comparison experiments on MSRA10K: (a) Original input images, and results of (b) scaling, (c) cropping, (d) TSC, (e) SC-IE, and (f) SC-OE.

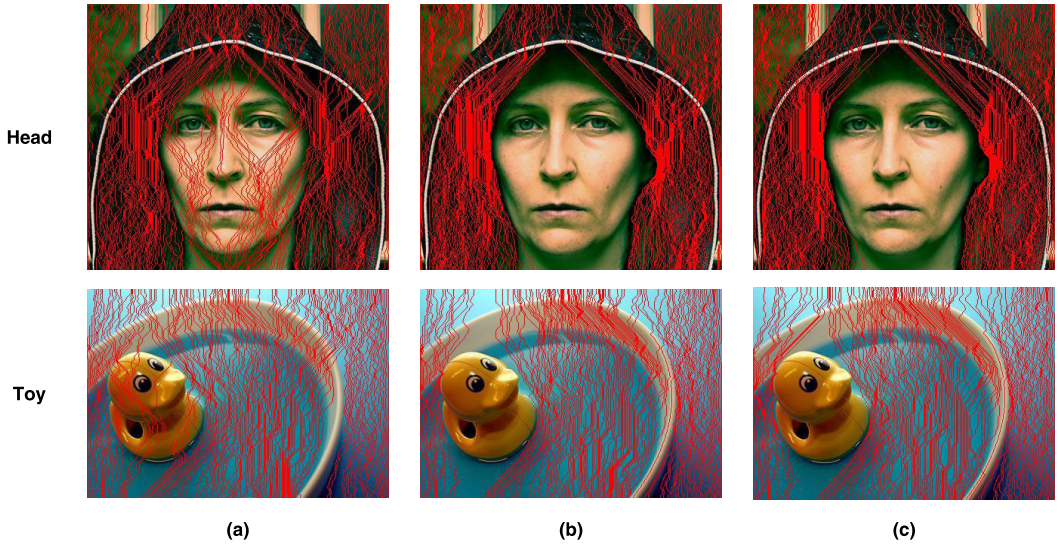

FIGURE 7. Experiments results of optimal seams on MSRA10K. Red lines are the removed seams of (a) TSC, (b) SC-IE, and (c) proposed SC-OE methods.

in columns (b) to (f) are the results of scaling, cropping, TSC, SC-IE, and the proposed SC-OE adaptation methods, respectively. Figure 7 depicts the optimal deleted seams of TSC, SC-IE, and the proposed SC-OE methods.

In Figure 6f, the face and duck areas are completely preserved, and the contour of the hat is smooth and natural. The image in Figure 6f is clearly more accurate than the other methods in Figures 6a–e.

The objective evaluation results of the two abdominal CT images in the MSRA10K data set are listed in Table 2. The average score of the proposed SC-OE on the two images of MSRA10K data set were 8.1 and 7.9 for Head and Toy, respectively, which are higher than the other methods. The proposed SC-OE algorithm is better than other methods, and the results of the proposed SC-OE are more in line with human visual requirements.

The reasons for the MSRA10K results are same as for the SLIVER07 data set. The scaling and cropping methods do not consider the importance of image content, which leads to an imbalance in the proportions of the face and duck areas in Figure 6b and information loss of the contour of hat area in Figure 6c. In Figure 6d, the TSC method only depends on an imprecise gradient map. The imprecise evidence results in the seams passing through the face and duck regions, as shown in Figure 7a. In Figure 6e, with the SC-IE method, the non-optimized energy map results in distortion of the edge

TABLE 2. Average scores of results for the MSRA10K data set.

Image	Average scores				
	Scaling	Cropping	TSC	SC-IE	Proposed SC-OE
Head	3.9	4.0	7.2	7.7	8.1
Toy	4.0	4.0	6.8	7.5	7.9

TABLE 3. Comparison of computational time of different methods.

Image	Size (pixels)	Optimal horizontal adaption percentage	Computational time (s)		
			TSC	SC-IE	Proposed SC-OE
CT-1	512 × 512	15%	22.212	22.673	22.749
CT-2	512 × 512	15%	22.465	22.883	22.973
Head	400 × 350	25%	13.543	15.253	15.323
Toy	400 ×277	25%	10.589	12.001	12.058

in unimportant areas due to the concentrated seams, as shown in Figure 7b. In Figure 6f, the proposed SC-OE method optimizes the energy map according to the content importance of the images and the contour characteristics in unimportant areas, and the optimal seams can evenly pass through the contour area in the non-salient region, as shown in Figure 7c. The proposed SC-OE is built on an precise importance map and contour-maintaining-based energy optimization. So, the visual effect of the proposed SC-OE method (Figure 6f) is better than the results of the other methods.

E. COMPUTATIONAL TIME

Since scaling and cropping do not consider the importance of image content, their implementations are faster in real time. The execution times of the other three methods are expressed in Table 3. TSC was quickest in the experiments, with little variation between the computational times of SC-IE and SC-OE. The proposed SC-OE method takes 2.4%, 2.3%, 13.1%, and 13.9% longer than TSC in the four experiments, as shown in Table 3.

The results can be explained by the main time-consumption bottleneck of three methods being the sub-procedure of forward seam carving. Because TSC only calculates the gradient map as the energy map, the method is faster. SC-IE uses the additional processes of saliency and edge detection, which requires more time. SC-OE is a little slower than SC-IE because the proposed SC-OE includes one more energy optimization procedure. Specifically, in the CT-1 and CT-2 experiments, saliency maps are generated by the morphological approach, which is more efficient than Cheng's method [29]. Thus, the time variation between SC-IE and TSC on CT-1 and CT-2 is less than the variation for Head and Toy.

IV. CONCLUSION

This paper proposes a contour-maintaining-based image adaptation method, called SC-OE, for an efficient ambulance ITS service. Firstly, the method combines weighted gradient, saliency, and edge maps into an importance map. Secondly, according to the slope and curvature of the edge in unimportant areas, serrated channels are set in the gentle edge area that can guide the optimal seams to evenly pass through edge areas. This can reduce the distortion and deformation and keep the original shape as much as possible. Finally, adaptation is conducted by forward seam carving. The computation time of the proposed SC-OE method is almost the same as TSC and SC-IE, but produces better visual effect performance than the other methods. The proposed SC-OE method is more suitable for offline or batch processing scenarios, which occur often in medicine and daily life. Further research is required to study more high-quality content-aware image adaptation methods and optimize the execution procedure to improve the efficiency and performance of the algorithms.

ACKNOWLEDGMENT

QingFang Liu, BaoSheng Kang, Keping Yu, Xin Qi, Jing Li, Shoujin Wang are co-first authors.

REFERENCES

[1] H.-A. Li, Z.-M. Du, J. Zhang, and Z. Li, "A retrieval method of medical 3D models based on sparse representation," *J. Med. Imag. Health Informat.*, vol. 9, no. 9, pp. 1988–1992, Dec. 2019, doi: 10.1166/jmihi.2019.2831.

[2] Z. Ning, Y. Li, P. Dong, X. Wang, M. S. Obaidat, X. Hu, L. Guo, Y. Guo, J. Huang, and B. Hu, "When deep reinforcement learning meets 5G vehicular networks: A distributed offloading framework for traffic big data," *IEEE Trans. Ind. Informat.*, early access, 2019, doi: 10.1109/tii.2019.2937079.

[3] Z. Ning, Y. Feng, M. Collotta, X. Kong, X. Wang, L. Guo, X. Hu, and B. Hu, "Deep learning in edge of vehicles: Exploring trirelationship for data transmission," *IEEE Trans. Ind. Informat.*, vol. 15, no. 10, pp. 5737–5746, Oct. 2019, doi: 10.1109/tii.2019.2929740.

[4] Z. Ning, P. Dong, X. Wang, J. Rodrigues, and F. Xia, "Deep reinforcement learning for vehicular edge computing: An intelligent offloading system," *ACM Trans. Intell. Syst. and Technol.*, vol. 10, no. 6, Dec. 2019, doi: 10.1145/3317572.

[5] Z. Ning, J. Huang, X. Wang, J. J. P. C. Rodrigues, and L. Guo, "Mobile edge computing-enabled Internet of vehicles: Toward energy-efficient scheduling," *IEEE Netw.*, vol. 33, no. 5, pp. 198–205, Sep. 2019, doi: 10.1109/mnet.2019.1800309.

[6] X. Wang, Z. Ning, X. Hu, L. Wang, L. Guo, B. Hu, and X. Wu, "Future communications and energy management in the Internet of vehicles: Toward intelligent energy-harvesting," *IEEE Wireless Commun.*, vol. 26, no. 6, pp. 87–93, Dec. 2019, doi: 10.1109/mwc.001.1900009.

[7] C. Chen, Y. Ding, X. Xie, S. Zhang, Z. Wang, and L. Feng, "TrajCompressor: An online map-matching-based trajectory compression framework leveraging vehicle heading direction and change," *IEEE Trans. Intell. Transp. Syst.*, early access, 2019, doi: 10.1109/tits.2019.2910591.

[8] C. Chen, D. Zhang, X. Ma, B. Guo, L. Wang, Y. Wang, and E. Sha, "Crowddeliver: Planning city-wide package delivery paths leveraging the crowd of taxis," *IEEE Trans. Intell. Transp. Syst.*, vol. 18, no. 6, pp. 1478–1496, Jun. 2017, doi: 10.1109/tits.2016.2607458.

[9] C. Chen, S. Jiao, S. Zhang, W. Liu, L. Feng, and Y. Wang, "TripImputor: Real-time imputing taxi trip purpose leveraging multi-sourced urban data," *IEEE Trans. Intell. Transp. Syst.*, vol. 19, no. 10, pp. 3292–3304, Oct. 2018, doi: 10.1109/tits.2017.2771231.

[10] K. Yu, S. Eum, T. Kurita, Q. Hua, T. Sato, H. Nakazato, T. Asami, and V. P. Kafle, "Information-centric networking: Research and standardization status," *IEEE Access*, vol. 7, pp. 126164–126176, 2019, doi: 10.1109/access.2019.2938586.

[11] X. Qi, Y. Su, K. Yu, J. Li, Q. Hua, Z. Wen, J. Lopez, and T. Sato, "Design and performance evaluation of content-oriented communication system for IoT network: A case study of named node networking for real-time video streaming system," *IEEE Access*, vol. 7, pp. 88138–88149, 2019, doi: 10.1109/access.2019.2925885.

[12] Y. Kim, S. Jung, C. Jung, and C. Kim, "A structure-aware axis-aligned grid deformation approach for robust image retargeting," *Multimedia Tools Appl.*, vol. 77, no. 6, pp. 7717–7739, Mar. 2018, doi: 10.1007/s11042-017-4674-1.

[13] S. Avidan and A. Shamir, "Seam carving for content-aware image resizing," *ACM Trans. Graph.*, vol. 26, no. 3, p. 10, Jul. 2007, doi: 10.1145/1276377.1276390.

[14] M. Rubinstein, A. Shamir, and S. Avidan, "Improved seam carving for video retargeting," *ACM Trans. Graph.*, vol. 27, no. 3, p. 1, Aug. 2008, doi: 10.1145/1360612.1360615.

[15] Q. Wang and Y. Yuan, "High quality image resizing," *Neurocomputing*, vol. 131, pp. 348–356, May 2014, doi: 10.1016/j.neucom.2013.09.032.

[16] Y. Zhang, Z. Sun, P. Jiang, Y. Huang, and J. Peng, "Hybrid image retargeting using optimized seam carving and scaling," *Multimedia Tools Appl.*, vol. 76, no. 6, pp. 8067–8085, Mar. 2017, doi: 10.1007/s11042-016-3318-1.

[17] Y. Guo, F. Liu, J. Shi, Z.-H. Zhou, and M. Gleicher, "Image retargeting using mesh parametrization," *IEEE Trans. Multimedia*, vol. 11, no. 5, pp. 856–867, Aug. 2009, doi: 10.1109/tmm.2009.2021781.

[18] J. Xu, H. Kang, and F. Chen, "Content-aware image resizing using quasi-conformal mapping," *Vis. Comput.*, vol. 34, no. 3, pp. 431–442, Mar. 2018, doi: 10.1007/s00371-017-1350-4.

[19] Y.-S. Wang, C.-L. Tai, O. Sorkine, and T.-Y. Lee, "Optimized scale-and-stretch for image resizing," *ACM Trans. Graph.*, vol. 27, no. 5, p. 1, Dec. 2008, doi: 10.1145/1409060.1409071.

[20] Z. Karni, D. Freedman, and C. Gotsman, "Energy-based image deformation," *Comput. Graph. Forum*, vol. 28, no. 5, pp. 1257–1268, Jul. 2009, doi: 10.1111/j.1467-8659.2009.01503.x.

[21] M. Rubinstein, A. Shamir, and S. Avidan, "Multi-operator media retargeting," *ACM Trans. Graph.*, vol. 28, no. 3, p. 1, Jul. 2009, doi: 10.1145/1531326.1531329.

[22] Y. Fang, Z. Fang, F. Yuan, Y. Yang, S. Yang, and N. N. Xiong, "Optimized multioperator image retargeting based on perceptual similarity measure," *IEEE Trans. Syst., Man, Cybern., Syst.*, vol. 47, no. 11, pp. 2956–2966, Nov. 2017, doi: 10.1109/tsmc.2016.2557225.

[23] C. Koch and S. Ullman, "Shifts in selective visual attention: Towards the underlying neural circuitry," *Matters of Intelligence*. Dordrecht, The Netherlands: Springer, 1987, pp. 115–141.

[24] X. Lu, J. Wu, X. Ren, B. Zhang, and Y. Li, "The study and application of the improved region growing algorithm for liver segmentation," *Optik*, vol. 125, no. 9, pp. 2142–2147, May 2014, doi: 10.1016/j.ijleo.2013.10.049.

[25] M. G. Linguraru, Z. Li, F. Shah, S. Chin, and R. M. Summers, "Automated liver segmentation using a normalized probabilistic atlas," *Proc. SPIE, Med. Phys.*, vol. 7262, Feb. 2009, Art. no. 72622R, doi: 10.1117/12.810938.

[26] H. Jiang, B. He, Z. Ma, M. Zong, X. Zhou, and H. Fujita, "Liver segmentation based on snakes model and improved growcut algorithm in abdominal CT image," *Comput. Math. Methods Med.*, vol. 2013, pp. 1–12, Jul. 2013, doi: 10.1155/2013/958398.

[27] L. Itti, C. Koch, and E. Niebur, "A model of saliency-based visual attention for rapid scene analysis," *IEEE Trans. Pattern Anal. Mach. Intell.*, vol. 20, no. 11, pp. 1254–1259, Nov. 1998, doi: 10.1109/34.730558.

[28] X. Hou and L. Zhang, "Saliency detection: A spectral residual approach," in *Proc. IEEE Comput. Soc. Conf. Comput. Vis. Pattern Recognit.*, Minneapolis, Minnesota, USA, Jun. 2007, doi: 10.1109/CVPR.2007.383267.

[29] M. Cheng, N. J. Mitra, X. Huang, P. H. S. Torr, and S. Hu, "Global contrast based salient region detection," *IEEE Trans. Pattern Anal. Mach. Intell.*, vol. 37, no. 3, pp. 569–582, Mar. 2015, doi: 10.1109/TPAMI.2014.2345401.

[30] J. Canny, "A computational approach to edge detection," *IEEE Trans. Pattern Anal. Mach. Intell.*, vol. 8, no. 6, pp. 679–698, Nov. 1986, doi: 10.1109/TPAMI.1986.4767851.

[31] C. Steger, "An unbiased detector of curvilinear structures," *IEEE Trans. Pattern Anal. Mach. Intell.*, vol. 20, no. 2, pp. 113–125, Feb. 1998, doi: 10.1109/34.659930.

[32] P. Sun, "Introduction to differential geometry of curves and surfaces in a four dimensional symplectic space," *Acta Math. Sinica*, vol. 4, no. 5, pp. 497–507, 1954.

[33] T. Heimann, B. van Ginneken, and M. Styner, "Comparison and evaluation of methods for liver segmentation from CT datasets," *IEEE Trans. Med. Imag.*, vol. 28, no. 8, pp. 1251–1265, Feb. 2009, doi: 10.1109/TMI.2009.2013851.

QINGFANG LIU received the M.S. degree in computer science and technology from Northwest University, Shaanxi, China, in 2009, where he is currently pursuing the Ph.D. degree.

Since 2017, he has been a Senior Engineer with the Information and Network Center, Training Center of China Post Group. His research interests include image processing, intelligent transportation, computer graphics and computer-aided geometric design, and virtual reality.

BAOSHENG KANG received the Ph.D. degree from Northwest Polytechnical University, Shaanxi, China, in 1991.

He is currently a Professor with the School of Information Science and Technology, Northwest University. He has authored more than 50 technical articles for conferences and journals. His research interests include image processing, computer graphics and computer-aided geometric design, and virtual reality.

KEPING YU (Member, IEEE) received the M.E. and Ph.D. degrees from the Graduate School of Global Information and Telecommunication Studies, Waseda University, Tokyo, Japan, in 2012 and 2016, respectively. He was a Research Associate with the Global Information and Telecommunication Institute, Waseda University, from 2015 to 2019. He is currently a Junior Researcher with the Global Information and Telecommunication Institute, Waseda University. He has hosted and participated in a lot of research projects, including the Ministry of Internal Affairs and Communication (MIC) of Japan, the Ministry of Economy, Trade and Industry (METI) of Japan, the Japan Society for the Promotion of Science (JSPS), the Advanced Telecommunications Research Institute International (ATR) of Japan, the Keihin Electric Railway Corporation of Japan, and the Maspro Denkoh Corporation of Japan. He is also the Leader and a coauthor of the comprehensive book *Design and Implementation of Information-Centric Networking* (Cambridge University Press, 2020). He was involved in many standardization activities organized by ITU-T and ICNRG of IRTF, and contributed to the ITU-T Standards "ITU-T Y.3071: Data Aware Networking (Information Centric Networking) Requirements and Capabilities" and "Y.3033-Data Aware Networking-Scenarios and Use Cases." His research interests include smart grids, information-centric networking, the Internet of Things, blockchain, and information security. He has had experience with editorial and conference organizations. He has served as the General Co-Chair and Publication Co-Chair of the IEEE VTC2020-Spring EBTSRA Workshop, the TPC Co-Chair of SCML2020, and the Session Chair of the ITU Kaleidoscope 2016. Moreover, he has served as a TPC member of the ITU Kaleidoscope 2020, IEEE VTC2020-Spring, IEEE CCNC 2020, IEEE WCNC 2020, IEEE VTC2019-Spring, ITU Kaleidoscope 2019, IEEE HotICN 2019, IEEE ICCC 2019, IEEE WPMC 2019, EEI 2019, and ICITVE 2019. He is also an Editor of the IEEE *Open Journal of Vehicular Technology* (OJVT).

XIN QI received the M.E. and Ph.D. degrees from Waseda University, Tokyo, Japan, in 2016 and 2019, respectively. He is currently a Research Associate with the Global Information and Telecommunication Institute, Waseda University. His research interest includes ICN and 3N for next generation communication systems.

JING LI received the B.E. degree in electronic information engineering from Nanchang University, China, in 2005, and the Ph.D. degree in electronic and electrical engineering from the University of Sheffield, U.K., in 2011. From 2011 to 2012, she was a Research Associate with the Department of Computer Science, University of Sheffield. She is currently an Associate Professor with the School of Information Engineering, Nanchang University. Her research interests include visual tracking, behavior recognition, and scene understanding in complex environments. She has authored or coauthored in various journals, such as the IEEE TRANSACTIONS ON INDUSTRIAL INFORMATICS, the IEEE TRANSACTIONS ON IMAGE PROCESSING, the *Information Sciences* (Elsevier), and so on.

SHOUJIN WANG is currently a Research Fellow of data science and artificial intelligence with Macquarie University, Sydney, Australia. His primary research interests include data mining, machine learning, and recommender systems.

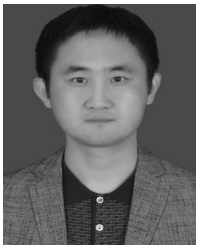

HONG-AN LI received the M.S. and Ph.D. degrees in computer science and technology from Northwest University, Shaanxi, China, in 2009 and 2014, respectively.

Since 2014, he has been an Associate Professor with the College of Computer Science and Technology, Xi'an University of Science and Technology. His research interests include computer graphics and computer-aided geometric design, virtual reality, and image processing.